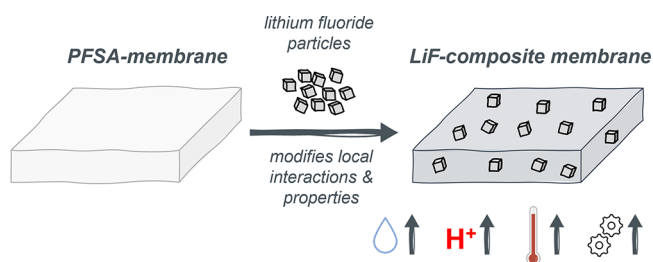# LiF@PFSA-Based Composite Membranes for PEM Fuel Cells at Intermediate Temperature Conditions

Maximilian Kutter,* Annika Hilgert, Maximilian Maier, Monja Schilling, Christopher R. Greve, Rameshwori Loukrakpam, Wiebke Hagemeier, Andreas Rosin, Mark Muggli, Eva M. Herzig, Roswitha Zeis, Thomas Böhm, Thorsten Gerdes, and Christina Roth

ABSTRACT: Polymer electrolyte membrane fuel cells (PEMFCs) operating at temperatures above 100 °C offer an interesting opportunity for heavy-duty applications. Especially for intermediate operating temperatures between 110 and 130 °C (IT-PEMFC), faster reaction kinetics, higher tolerance to fuel impurities, and water flooding as well as improved heat management of the fuel cell system have been observed. Perfluorosulfonic acid-based membranes (PFSAs) can be modified by incorporating additives or (nano)particle filler systems to improve their thermal and mechanical stability, proton con-

ductivity, and long-term performance at these increased temperatures. Here, we investigate the effect of lithium fluoride particles embedded in PFSA membranes on their water retention behavior as well as on membrane durability in single-cell tests at elevated PEMFC operating temperatures of up to 120 °C. The lithium fluoride nanoparticle-modified membrane shows increased cell performance under both standard and intermediate temperature conditions. The observed performance boost can be explained by an increased mechanical stability at elevated temperatures of the membrane, due to stabilizing hydrophobic and hydrophilic domains, and an increased water uptake and storage capability, especially at low humidity levels during full cell operation. We propose that the nanoparticles adsorb water molecules by hydrogen bond formation, thus enhancing proton conductivity even at high temperatures resulting in these increased full cell performances of the LiF@PFSA-based composite membrane.

KEYWORDS: composite membranes, metal fluorides, intermediate temperature PEM fuel cells, in situ Raman, SAXS study, water retention

1. INTRODUCTION

Polymer electrolytes are essential components for the operation of electrochemical energy conversion systems, such as fuel cells and electrolyzers, due to their function as ion-conducting separators between the electrodes. In fuel cell systems, polymer electrolytes are benchmarked against proton-conductive mostly perfluorosulfonic acid (PFSA) polymers, such as Nafion (Chemours), and further developed short-side chain (SSC) ionomers from e.g. Solvay or 3M. PFSA ionomers show good chemical and mechanical stability and already high proton conductivity at standard operating temperatures of 60 to 80 °C.[1] However, their conductivity is strongly linked to the water content of the hydrophilic channels in the membrane, with a higher water content leading to enhanced proton transfer.[2] As the membrane dries out at higher temperatures or lower relative humidity, the hydrophilic channels will start to collapse, resulting not only in reduced conductivity, but also in decreased mechanical stability. For this reason, the operating temperature of the low temperature PEM fuel cell (LT-PEMFC) is limited to temperatures below the boiling point of water, which has various disadvantages. Due to this limitation a complex water management system is required to ensure sufficient humidification of the membrane and removal of the liquid product water.[3] Furthermore, because of the low operating temperature, the gases used must not contain any impurities like CO, as this would poison the catalyst and lead to a severe loss of performance.[4,5] One way to circumvent these disadvantages is to increase the operating temperature of the system to temperatures above 100 °C. This leads to faster reaction kinetics, better heat dissipation, and easier water management, simplifying system design.[4,6] However, some issues regarding durability and performance, particularly lower long-term stability at increased temperatures, are still unresolved.[7,8]

Several promising strategies to increase the performance of PEMFCs at low relative humidity and temperatures above 100 °C have been developed over the last decades and reported in the respective literature.[9] Some approaches focused on modifying existing ionomers by cross-linking different polymeric materials to improve their mechanical and chemical stability.[10,11] Others focused on the design of cheaper and highly conductive sulfonated aromatic/hydrocarbon-based membranes (e.g., SPEEK or Pemion) showing high proton conductivity and good fuel cell performance as shown by various groups.[12−14] In the publication by Shang et al.[12] poly(phenylene sulfonic acid)-expanded polytetrafluoroethylene composite membranes were obtained by thermal cross-linking and tested at low humidity conditions. These demonstrated exceptionally high performances at 80 °C and 30% RH, but were not studied for their long-term performance. Since the development of the polybenzimidazole (PBI) membrane doped with phosphoric acid (PA) by Litt and Savinell[15] in the mid-1990s, PA-doped membrane systems have demonstrated good fuel cell performance, particularly under anhydrous conditions and even at temperatures above 140 °C.[15−18] In 2023, Lim et al.[19] evaluated an ion-pair based membrane, focusing on its ability to retain phosphoric acid under various conditions. The membrane demonstrated superb performance in phosphoric acid retention during a series of long-term accelerated stress tests, while also achieving excellent peak power density (PPD). Another research direction in polymer engineering is the incorporation of inorganic additives or filler particles into the PFSA polymer matrix to improve its water retention. Especially the latter strategy leads to higher mechanical stability and, therefore, better performance at elevated temperatures. These fillers can consist of various metal oxides (e.g., silicon, titanium, aluminum or zirconium oxides),[20,21] metal phosphates (e.g., zirconium phosphates)[22,23] or binary/functionalized additives (e.g., TiO_2−SO_4, ZrO_2/SiO_2).[24,25] where the inorganic filler systems primarily increase the water uptake and retention of the membrane at elevated temperatures by a direct interaction with the water molecules.[20] This increase in water content directly corresponds to faster proton transfer.[9] Furthermore, an interplay between different parameters is crucial as described by Di Noto et al.[26] Proton migration in composite membranes strongly depends on formed water channels, hydrophilic clusters and the formation of additive/SO_3^- species. These microstructural properties can be studied by scattering techniques, such as small-angle X-ray and neutron scattering (SAXS, SANS). Especially, investigations under real temperature and humidity conditions offer access to information that can help to improve the membrane performance in the realistic and application-relevant setting. Based on previous studies, various morphology models, such as the cluster network model by Gierke and co-workers,[27,28] the core−shell model,[29] the rod-like model[30] and (parallel) cylindrical model.[31] have been proposed. All models hold the SO_3^- groups responsible for forming water channels, with their morphology changing as a function of water content. Since the transport properties of composite membranes strongly depend on the additive/SO_3^- species and therefore the resulting water channels, the study of phase separation and microstructure can offer further information on their performance related effects. In addition, matrix structure, side chain and backbone formation also play a significant role in membrane properties. The matrix's mechanical stability largely depends on the formation of the crystalline polytetrafluoroethylene (PTFE)-based backbone.[32] The membrane's performance and long-term stability may be negatively affected if its evolution is disturbed by too high amounts or inappropriate additives. A high filler content can weaken the matrix structure, resulting in a loss of mechanical stability and brittle membranes.

A limiting factor for the commercialization of composite membranes, which is rarely discussed in the literature, is the complex and cost-intensive synthesis of the additive materials. The complex fabrication of nanosized metal oxides and binary or functionalized additives by sol−gel or wet synthesis routes is a major drawback in the commercialization of IT-PEMFCs. Metal fluoride byproducts, which can arise in fluorine chemistry, can solve this bottleneck issue. First indications on how operation temperatures of PEM fuel cells can be increased by adding fluoride salts into the electrolyte were reported in the patent by Moszczynska et al.[33] and Muggli et al.[34]

This work presents a strategy to enhance water retention in PFSA membranes for IT-PEMFC applications by incorporating lithium fluoride particles into the ionomer matrix. Two different types of lithium fluoride, a commercially available lithium fluoride (LiF(c)) and ball-milled lithium fluoride (LiF(m)), were investigated, aiming to analyze the influence of particle size and morphology. The structural and mechanical properties of the obtained composite membranes were studied by different analytical techniques such as dynamic mechanical analysis (DMA), thermogravimetric analysis (TGA), dynamic vapor sorption (DVS), IR, Raman and SAXS. In addition, conductivity measurements and fuel cell tests have been used to test the membranes under realistic conditions and compare their performances.

2. EXPERIMENTAL SECTION

2.1. Lithium Fluoride Preparation. The lithium fluoride particles were wet-milled using a planetary ball mill (Fritsch, Germany) equipped with a zirconium oxide container and 40 zirconium oxide milling balls (10 mm diameter) similar to a previously reported synthesis method by Wall et al.[35] The commercially available lithium fluoride (*BioUltra*, Sigma-Aldrich) with an original particle size of 1 to 10 μm was ball-milled in 2-propanol, in a 1:3 mass ratio. The ball mill was operated for 20 h at 250 rpm rotational speed. The remaining solid was dried at 60 °C overnight.

2.2. Preparation of Composite Membranes. 0.5 g of the 3M-800EW ionomer was first suspended in 4.5 g 1-propanol/water solution (95/5 w/w) and stirred for 36 h. Subsequently 6−20 wt % of the lithium fluoride filler (referred to the ionomer content) was dispersed with 1 mL of 1-propanol for 30 min in an ultrasonic bath to break up possible agglomerates. Afterward it was added to the polymer dispersion and stirred, until a homogeneous suspension was obtained. The additive-polymer slurry was degassed on a rotary evaporator and subsequently poured onto a plate covered with Kapton film, which was placed on a Coatmaster 509 MC doctor-blading table from ERICHSEN GmbH & Co. KG. In the casting process, the doctor blade was pulled over the dispersion with a gap height of 650 μm and a speed of 10 mm s^{-1}, resulting in a uniform 30−35 μm composite membrane. After the doctor blade coating, the membrane was dried for 15 min at room temperature, before it was further dried at 80 °C for 30 min in a drying oven. After undergoing thermal annealing at 180 °C for 10 min, the membranes were washed in a 5% hydrogen peroxide solution for 1 h, followed by protonation in a 1.5 M sulfuric acid solution for 3 h at room temperature. The CCM fabrication steps can be found in the Supporting Information.

2.3. Powder X-Ray Diffraction (PXRD). The crystallite sizes of the lithium fluoride were determined by powder X-ray diffraction

(PXRD) on a Philips X'Pert System MPD diffractometer using Cu–K_α radiation. The diffraction patterns were recorded in a 2θ range from 10° to 90°. The diffractograms were evaluated and the crystallite sizes were calculated by the Scherrer equation, using the X'Pert HighScore software from Malvern Panalytical. Before each measurement the sample was finely ground and equally distributed on the sample carrier. All measurements were performed in air at room temperature and ambient pressure.

2.4. Brunauer–Emmett–Teller Analysis (BET). The Brunauer–Emmett–Teller (BET) analysis was used to determine the specific surface area of the lithium fluoride particles. The measurements were performed on an ASAP 2010 model from Micromeritics Instrument Corporation. Before every measurement, the samples were dried and degassed at 80 °C in high vacuum for several hours to remove surface contaminants and water. The measurements were performed with nitrogen as adsorptive gas at 77 K.

2.5. Dynamic Light Scattering (DLS). The particle size distribution of the lithium fluoride particles was analyzed on a particle size analyzer PSA 1190 L/D from Anton Paar. The particles were dispersed in water by sonication for 1 h and measured at room temperature. The particle size distribution and the d10, d50 and d90 values were calculated from the total sum curve of this distribution using the Rosin-Rammler method.

2.6. Scanning Electron Microscopy (SEM). Cross-section SEM pictures of the membranes were obtained using a FEI Quanta FEG 250 scanning electron microscope (SEM). The membrane cross sections were prepared by breaking the membranes in liquid nitrogen. After preparation, the samples were sputter-coated with gold to avoid charging artifacts.

2.7. Fourier-Transform Infrared Spectroscopy (FTIR). Infrared absorption spectroscopy measurements were performed on a Vertex 70 FTIR-ATR spectrometer from Bruker equipped with a DTGS detector (RT DLaTGS) and a single reflection diamond ATR accessory. The spectra were acquired by accumulating 16 scans at a spectral resolution of 1 cm^{-1} from 400 to 4000 cm^{-1} at room temperature.

2.8. Thermogravimetric Analysis (TGA). Thermogravimetric analysis (TGA) was performed on a Netzsch STA 449 C machine using a heating rate of 5 K min^{-1} in nitrogen atmosphere. The Software Proteus from Netzsch was used for data evaluation.

2.9. Dynamic Mechanical Analysis (DMA). The mechanical properties of the membranes were studied on an MCR 702e MultiDrive dynamic mechanical analyzer (Anton Paar, Germany). The samples with an area of 3.5 × 0.8 mm were placed between the tension clamps and tested at a fixed frequency of 1 Hz and an amplitude of 10 μm. The temperature ramp was set from room temperature up to 150 °C at a rate of 2.5 K min^{-1}. From the collected data tan(δ) values were calculated as a function of temperature.

2.10. Small Angle X-Ray Scattering (SAXS). Small angle X-ray scattering measurements were performed using a Xeuss 3.0 (Xenocs, France) equipped with a copper source (λ = 1.5418 Å). Scattering images were detected on an Eiger2 R 1 M detector (Dectris, Switzerland) with 1028 × 1062 pixels and a pixel size of 75 μm × 75 μm located 0.3 m from the sample as obtained from AgBeh calibration. The beam size was adjusted to 0.5 mm × 0.5 mm, and each sample was measured for 2 h in ambient atmosphere, with single-image exposure times of 30 min. The measured single SAXS images were averaged, 1D cuts extracted and background corrected for air scattering and peak positions were determined by fitting each peak profile with a local background and a Gauss function using XSACT 2.0 (Xenocs, France).

2.11. Dynamic Vapor Sorption (DVS). Dynamic vapor sorption (DVS) measurements were performed on a Q5000 Sorption Analyzer (TA Instruments, precision ±0.01%) to study the water uptake of the membranes from the gaseous phase. Approximately 10 mg of the membrane were dried at 80 °C for 2 h prior to each measurement. The measurement protocol included a second drying step at 60 °C for 300 min to remove the remaining water, followed by sorption and desorption isotherms at 25 °C. The relative humidity (RH) was increased and decreased stepwise in 10% steps and isotherms were

recorded between 0% and 90% RH. To ensure equilibrium, the RH was kept between 0% and 50% RH for 60 min, 60% RH for 100 min, 70% and 80% RH for 120 min, and 90% RH for 180 min. Water uptake and water content were calculated using equations S1 & S2 respectively.

2.12. In-Situ Raman Spectroscopy. The Raman measurements were performed with a WITec alpha 300 RA (WITec, Germany) confocal Raman microscope. A laser at a wavelength of 532 nm was employed as the excitation source at a power of 40 mW. A dedicated home-built sample holder was used for in situ measurements in an aqueous environment. The signal was collected with a Zeiss W Plan-Apochromat 63x/1.0 objective and detected with a WITec UHTS 300 VIS spectrometer consisting of a Peltier-cooled back-illuminated EMCCD-camera (1600 pixel) and a 600 grooves mm^{-1} optical grating. The membranes were put in deionized water for at least 1 h prior to the Raman measurements to reach a sufficient level of hydration.

Five spectra with an integration time of 5 s each were accumulated to obtain a single Raman spectrum. For confocal through-plane scanning, the integration time was set to 20 ms per point with an axial step interval of 1 μm. The software WITec Project FIVE+ was employed to subtract the signal background from the raw spectra. The shape-based algorithm with a shape size of 400 and a noise factor of 1 was used. All further data processing steps were performed with custom-built MATLAB scripts (MathWorks, USA).

The water signal over depth was obtained by integrating the spectral area under the ν_s(O–H) (3000 to 3700 cm^{-1}) peak at every z-position of the through-plane scan. The details of this method were reported elsewhere by Peng et al.[36] A linear corrective function was implemented to correct scattering and absorption losses within the membrane so that the Raman signal of water above and beneath the sample was normalized to equal intensity levels. By calculating the ratio of the spectral intensities of the water signal within the membrane and the signal of pure water, the water volume fraction Φ_V was calculated according to[36]

$$\Phi_V = \frac{N_{sorbed}}{N_{pure}} = \frac{\rho_{sorbed}}{\rho_{pure}} = \frac{S_{sorbed}}{S_{pure}} \tag{1}$$

where ρ is the density (g m^{-3}) of water within the probed volume, N the number of molecules in the focal volume, and S the integrated signal of the Raman band.

The equivalent weight (EW) of the membranes was quantified by a device-specific calibration curve. The calibration for the EW was obtained by acquiring the Raman spectra of the 3M ionomer for four different EWs (670, 725, 800, and 980 g mol^{-1}). A detailed description of the technique and how to determine the device and PFSA-specific calibration curve can be found for Nafion and other SCC ionomers in the literature.[37,38] Once the calibration curve was obtained, the EW of an arbitrary 3M ionomer membrane sample could be quantified by acquisition of a single Raman spectrum.

2.13. Proton Conductivity Measurements. The ionic conductivity of the membranes was determined by in-plane conductivity measurements using impedance spectroscopy. The measurements were conducted in an in-house built measuring chamber under controlled temperature and humidity. The measuring clamp system was based on a commercial BekkTech cell. A detailed description of the setup is given by Heimerdinger et al.[39] The membranes were cut into rectangular pieces (dimensions: 1 cm × 2 cm) and placed between the clamps. The experiments were performed at a constant dew point of 70 °C and an increasing chamber temperature from 70 to 130 °C in 20 K steps, resulting in four operating conditions. An equilibration time of 2.5 h was set for each temperature step. The analyzing frequency range was from 1 MHz to 20 Hz with an amplitude of 20 mV controlled by a Hewlett-Packard HP 4284A LCR meter.

2.14. Single Cell Tests. Low temperature (LT) and intermediate temperature (IT) PEM fuel cell tests were performed on a Horiba-FuelCon Evaluator-C50-LT in an in-house built single cell with an active cell area of 9 cm^2 at two different temperatures (80 and 120

°C). Control and regulation of the media supply as well as monitoring of the cells was performed using the Testwork software. All cell tests were carried out in H_2-air mode.

For the break-in procedure, cell was heated to 45 °C. The gases were set to 85 °C and 20% RH by constant flow rates of 0.5 l min^{-1} on the anode and 1.5 l min^{-1} on the cathode side. After the cell reached a steady state, a constant current of 0.11 A cm^{-2} was applied for 3 h. Afterward, the cell temperature was increased to 80 °C with 20% RH and three galvanostatic polarization curves were recorded with increasing current steps (hold for 2 min) from OCV to a potential limit of 0.2 V. After the conditioning steps, polarization curves, high frequency resistances (HFRs) and open circuit voltage tests were performed for each operating condition. Further information and test parameters can be found in the Supporting Information (Figure S5, Tables S4, and S5).

3. RESULTS AND DISCUSSION

This work compares two different lithium fluoride additives incorporated into the ionomer matrix for their application in IT-PEM fuel cells. The additive systems used are commercially available lithium fluoride (LiF(c)) and lithium fluoride ground by a wet-milling process (LiF(m)), which are incorporated into a dispersion of an SSC ionomer with an equivalent weight of 800 g mol^{-1} produced by 3M. The resulting composite membranes have been investigated and compared to a nonmodified pristine membrane (henceforth called 800EW).

3.1. Characterization of Lithium Fluoride Particles.
The XRD patterns of the commercial and the milled lithium fluoride are presented in Figure 1(a). Both patterns show a
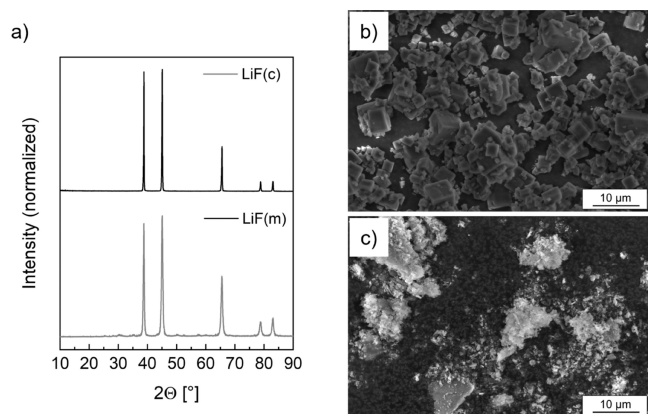

Figure 1. XRD patterns of the commercial (LiF(c)) and the ball-milled lithium fluoride (LiF(m)) (a), SEM images of the commercial (b) and the ball-milled lithium fluoride particles (c).

crystalline structure, identical griceite phase and the reflections can be assigned to LiF (ICDD-PDF-4−2020−00−004−0857). The reflections showed a broadening from LiF(c) to LiF(m), which indicates reduced particle sizes due to the milling process. The crystallite sizes were determined by the Scherrer equation which resulted in a mean crystallite size of 52 ± 3 nm for the as-received sample and 16 ± 1 nm for the treated sample.

Figure 1 also shows exemplary SEM pictures of both lithium fluoride powders in direct comparison. Figure 1(b) shows microcubes with an edge length between 1 and 10 μm. The cubic shape is reported as the typical morphology of lithium fluoride.[40] Figure 1(c) shows the lithium fluoride particles after wet-milling. A significant structural change can be observed. The particles have a more irregular appearance with smaller particle sizes which corresponds well to the XRD pattern. Sizes

calculated by the SEM pictures vary in the range of 100 nm to 10 μm.

These results are in good agreement with the DLS analysis. The respective d10, d50 and d90 values are shown in Table S1. The d50 value decreased from 7 to 0.65 μm for the treated LiF. Due to a significant tendency toward agglomerate formation of the milled particles, the observed sizes were slightly shifted to higher values.

Accordingly, the specific surface area of the treated lithium fluoride powder, expressed by the BET value, increased from 1.3 m^2 g^{-1} to 21.8 m^2 g^{-1} after milling.

3.2. Characterization of the Composite Membranes.
Composite Membrane Morphology. All tested composite membranes had an additive loading of 10 wt % with respect to the ionomer weight. The actual equivalent weight was verified by titration (Table S2). The optimal additive loading was obtained with the help of a water uptake and conductivity study shown in Figure 2 & Figure S3.

Figure 2(a) shows the water absorption data for the 800EW reference membrane and LiF(c) composite membranes with additive concentrations ranging from 6 wt % to 20 wt %. The comparison reveals a gradual increase in water absorption with increasing additive concentration until the optimum additive loading of 10 wt % is reached. Further increases in additive loading result in a steady decrease in water absorption. We conclude that excessive additive loading will disrupt the formation of the desired membrane structure, leading to improper formation of hydrophilic clusters and water channels, while also blocking these channels. On the other hand, at a lower concentration of 6 wt % LiF(c), the membrane's properties will not be significantly modified, the structural properties of an unmodified membrane retained and the interaction of the polar additive with water molecules through hydrogen bonding only minimally affected.

These findings are also reflected in the conductivity measurements (Figure 2(b)). A comparison across additive concentrations shows that a high loading, such as 12 wt %, results in a reduced conductivity in the 90 to 130 °C temperature range. At this concentration, a critical threshold is likely to be reached in terms of contact points and interaction between particles and ionomer, beyond which additional LiF particles no longer enhance proton transport at the interface and may even reduce thermal stability.

The morphology of the LiF composites was studied by SEM. The cross sections shown in Figure 3 demonstrate the incorporation of the particles into the polymer matrix. The LiF(c) modified composite shows cubic fracture patterns (Figure 3(a)), whereas the milled-LiF filler membrane exhibited round fracture patterns originating from the LiF(m) particles (Figure 3(b)). Further cross section images of the composite membranes at higher magnifications are shown in the Supporting Information (Figures S1 and S2).

Thermo-mechanical Analysis (TGA/DMA). The results of the TGA are displayed in Figure 4(a). All membranes show the characteristic degradation behavior for 3M membranes. An initial weight loss can be seen between room temperature and 100 °C followed by a constant weight loss between 100 °C and roughly 300 °C which can be attributed to the loss of initially bound water (~5 wt %) (I). The typical degradation of the side chain is observed for the unmodified membrane (800EW) at 320 to 325 °C by losing the sulfonic acid groups (II).[41] The lithium fluoride modified membranes showed no significant improvement in thermal degradation behavior. We did not see
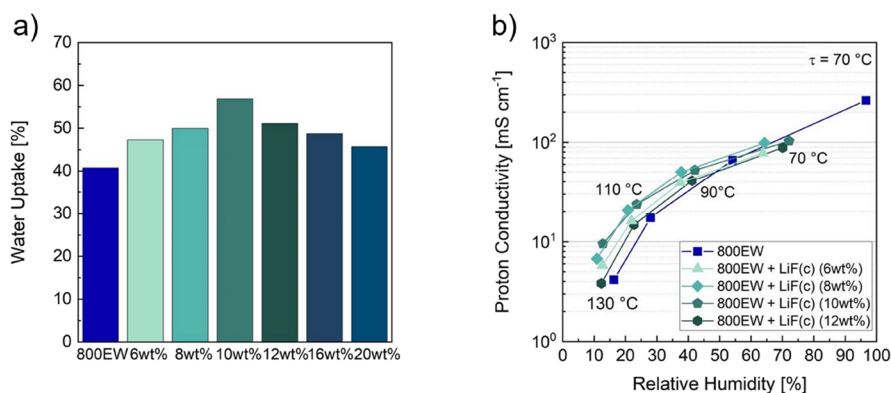
Figure 2. Results of the weight-dependent water absorption tests of the 800EW membrane and various LiF(c) composite membranes at 25 °C (a) and proton conductivity measurements of the 800EW and the LiF(c) composite membranes with various filler concentrations at different temperatures and relative humidity (b). A clear assignment of the measured conductivities to the corresponding temperatures can be found in SI: Figure S4.
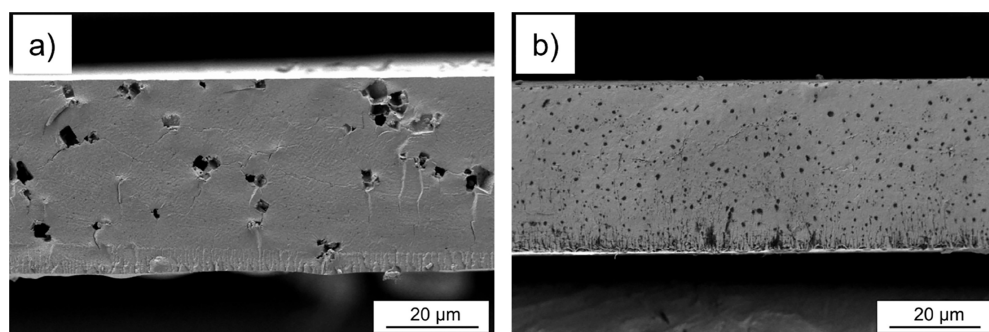

Figure 3. Cross section SEM images of the LiF(c) composite membrane (a) and the LiF(m) composite membrane (b).

Figure 4. TGA profiles (a) and temperature-dependent tan(δ) of the 800EW membrane and the LiF(m) composite membrane measured with DMA (b).

any thermal stability changes as reported by Jalani et al.[20] or Deng et al.[42] They reported that inorganic additives (SiO_2 or ZrO_2) incorporated in Nafion shift the composite membrane's thermal degradation behavior to higher values. The weight loss detected at 380 °C (III) is due to the decomposition of the remaining polymer side chain. The degradation of the PTFE backbone occurs between 440 and 530 °C (IV).[41,43] The thermal stability of the unmodified membrane was similar to the LiF modified membranes.

The DMA results for the modified and unmodified membranes are presented in Figure 4(b). The glass transition temperatures (T_g) were obtained from the tan(δ) peak. The T_g of the unmodified PFSA membrane can be observed at a temperature of 122 °C, which is in good agreement with literature values,[44] whereas the LiF@PFSA membrane reached a temperature of around 129 °C. Interestingly, no change in the loss tangent values can be observed, which indicates that the mobility of the backbone is not hindered due to the presence of the additive. Indeed, the results show that the composite material has a higher thermo-mechanical stability.

Vibrational Spectroscopy (IR/Raman). Vibrational spectroscopy was used to analyze structural changes, such as side chain cleavage or decomposition due to the presence of the additives. Figure 5(a) shows the IR-spectra of the 800EW membrane and the modified 800EW membrane. The spectrum of the unmodified membrane shows the expected vibrations for
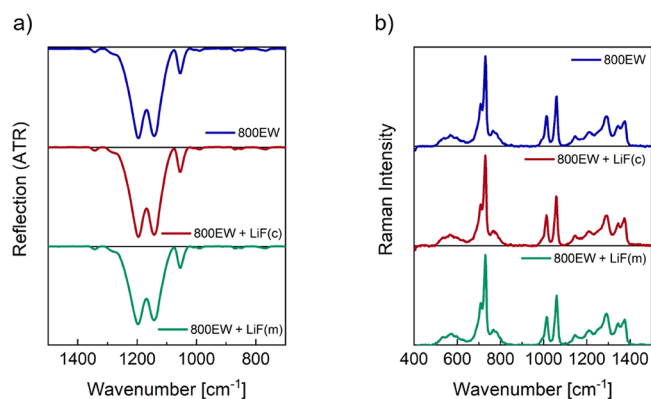
Figure 5. IR spectra (a) and Raman spectra (b) of the 800EW membrane, the LiF(c) and the LiF(m) composite membrane.

the functional groups C−F, C−O−C, and −SO$_3$H.[45] For the 3M-800EW ionomers, the bands at 1196 and 1142 cm^{-1} can be assigned to PTFE. These correspond to the antisymmetric ν_a(C−F)$_{bb}$ vibrations of the C−F bonds.[46] Furthermore, these peaks overlap with the ν_a(S−O) vibration as well as the ν(C−C) skeletal vibrations of the side chains and the PTFE backbone.[47] The symmetric stretching vibration ν_s(S−O) at 1055 cm^{-1} can be assigned to the sulfonic acid group. The same mode can also be found in the IR spectra of Nafion or Aquivion. The peak at 989 cm^{-1} can be attributed to the C−O−C bond between the backbone and the side chain.[34,48] The peak at 1342 cm^{-1} is often described in the literature as the symmetric stretching vibration of the ν_s(C−C) bond.[46] The spectrum of the lithium fluoride membrane shows the same vibrational modes as the unmodified membrane.

Maier et al.[38] analyzed the Raman signal of the 3M ionomer and associated Raman bands with characteristic bonds of the ionomer by evaluating the differences of the Raman spectra for Nafion, 3M and Aquivion and correlating them with the distinct chemical composition of the different ionomers. The peaks are either associated with the PTFE backbone or the side chain.[36,37,46,49,50] The most intense peak at 730 cm^{-1} stems from the PTFE backbone and is associated with the symmetric stretching ν_s(C−F)$_{bb}$.[46] The side chain-related bonds ν_s(C−O−C) and the ν_s(S−O) are assigned according to literature to the peaks at 1017 and 1061 cm^{-1}.[36,38,46] The third prominent side chain associated peak at 768 cm^{-1} has been either associated with the ν_s(C−S) bond,[50] or with the symmetric

vibration ν_s(C−F)$_{sc}$ of the C−F bonds in the side chain.[36−38] The peak at 768 cm^{-1} was attributed to the ν_s(C−F)$_{sc}$ vibration, as the spectral area is lower compared to the Raman spectrum of Nafion. Therefore, the peak area is in accordance with the lower amount of C−F bonds in the side chain of the 3M ionomer. The peak at 711 cm^{-1} was attributed to the ν_s(C−S) stretching.[38] The Raman spectra of the modified and pristine membranes are identical in spectral intensity and position for all backbone and side chain-related modes. The spectral ratio of the ν_s(S−O) and ν_s(C−F)$_{bb}$ peaks was used to quantify the EW of the pristine and a modified membrane (see section 2.13). The evaluation yielded an EW of 819 ± 15 g mol^{-1} for the pristine membrane, 832 ± 15 g mol^{-1} for the LiF(c) and 820 ± 15 g mol^{-1} for the LiF(m) modified membrane. Thus, no significant change in EW by modifying the 3M-800EW with LiF additive can be observed within the error margins of the method. In brief, the spectroscopic analysis demonstrates that LiF particle incorporation into the 3M ionomer membranes does not alter their chemical fingerprint.

Water Uptake. In this study, the water uptake of the membranes was investigated by three different techniques. The total water uptake was studied by soaking the membranes in liquid water, the uptake from water vapor by dynamic vapor sorption (DVS), and the water volume fraction of the membranes by in situ Raman measurements. All methods are widely used in literature.[51] However, investigating the water uptake behavior by DVS is closest to the fuel cell operating conditions.

In general, adding LiF increases the water uptake of the membranes. In the total water uptake studies, the water sorption could be increased by 15% for the LiF(c) and 16% for the LiF(m) doped one, respectively (Table S2).

The data from DVS are shown in Figure 6. The water uptake vs time profiles reveal that the weight changes, which correspond to the water uptake, are slightly increased using commercial and milled LiF, especially at high RH. The LiF(c) membrane showed the highest water sorption compared to the pristine membrane. The same trend can be seen in Figure 6(b) where sorption isotherms describe the water uptake behavior. Here, the water content is presented as a function of water activity (λ), calculated using equation S2 (see SI). At low RH, the isotherms of all investigated membranes show similar behavior. However, the LiF functionalized membranes adsorb slightly more water at higher RH (>70% RH). This behavior
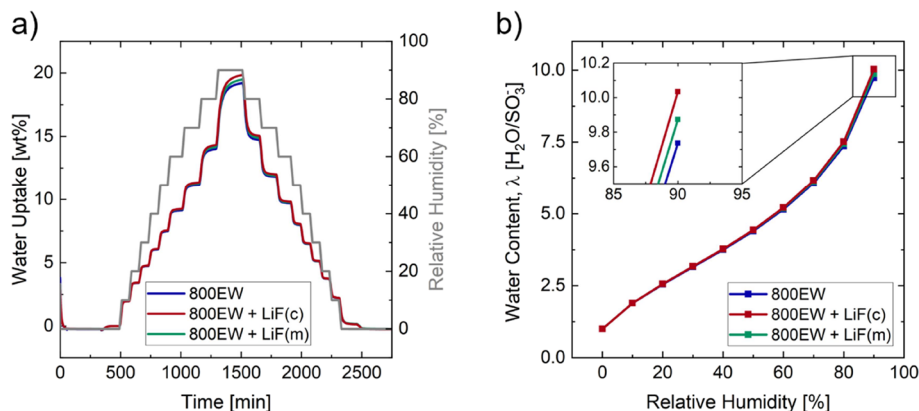

Figure 6. Time-resolved DVS profiles (a) and sorption isotherms of the 800EW membrane, the LiF(c) and the LiF(m) composite membrane at 25 °C (b).
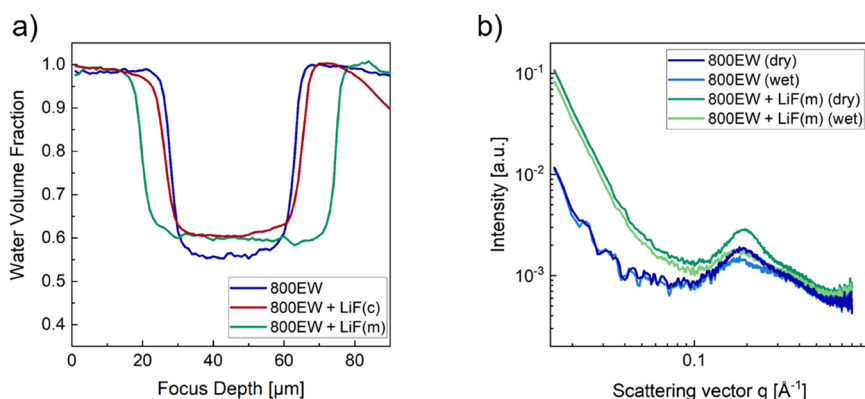
Figure 7. Water volume fractions of the 800EW membrane, the LiF(c), and the LiF(m) composite membrane (a). The water volume fraction was determined by confocal Raman microscopy and calculated according to eq 1. The spectral area of the $\nu_s(O-H)$ peak was used to determine the Raman signal of pure and sorbed water over the focus depth in through-plane scans. Ionomer peaks of 800EW and the LiF(m) composite membrane at dry conditions and in liquid water at 25 °C determined from in situ SAXS spectra (b).

could potentially result from an enhanced uptake of "free/freezable" water in the hydrophilic domains.[44] The results from the DVS tests follow the same trend for the total water uptake, as discussed before.

The water volume fraction was additionally measured in situ over the thickness of the pristine and modified 3M-800EW membrane using Raman spectroscopy. Confocal through-plane scans were performed to analyze the WU of the membranes in liquid water (Figure 7(a)). The data of all 800EW membranes present a uniform water uptake within the membrane, with a higher water content for the modified membranes. The average water volume fraction of the modified membranes is 60% for the LiF(m) additive, and 61% for the LiF(c), while the pristine membrane only reached an average water volume fraction of 56%. This corresponds to hydration numbers of $\lambda = 33$, $\lambda = 35$, and $\lambda = 29$ [H_2O]/[SO_3H], respectively. The higher water volume fraction and hydration number for the modified membrane corroborate the proposed better hydrophilic behavior of the LiF nanoparticles and are in line with the gravimetric determination of the WU.

SAXS measurements were used to analyze the microstructure and the effect of water uptake on the membranes in either a dry or static wet state. Especially the changes in the composite membrane's morphology due to the incorporation of the LiF nanoparticles and their influence on hydration and water retention have been studied. In a typical SAXS pattern three different characteristic features (peaks) can be observed, due to the different electron densities of the ionomer structure: the ionomer peak, the matrix knee and an upturn in the low q-region at values smaller than 0.04 Å^{-1}. The peak at values of q > 0.1 Å^{-1} can be attributed to the so-called ionomer peak representing the extent of the separation of hydrophilic and hydrophobic phases. The matrix knee upturn commonly observed between q = 0.04−0.08 Å^{-1} arises from the scattering of the crystalline PTFE backbone.[52,53] The upturn at even smaller q-values can be attributed to incorporation of larger structures or particles in the ionomer cluster.

The SAXS patterns of the pristine and the modified membrane in a dry and static wet state respectively, are presented in Figure 7(b). Surprisingly, all collected SAXS data show only two of the three expected features, namely the ionomer peak and the low q-upturn. The matrix knee is barely discernible, in contrary what was previously observed for 3M ionomers with low EWs by Liu et al.[54] Comparing the dry

800EW and the LiF(m) modified membrane, a shift of the ionomer peak from q = 0.183 Å^{-1} to q = 0.193 Å^{-1} can be observed, indicating that the additive affects the phase separation. Calculating the D-spacing,[54] defined as $2\pi/q$, with these peak positions, the distance between the hydrophilic and hydrophobic phases decreases slightly from 34.3 to 32.5 Å with the LiF(m) doping (Table S3), indicating an interaction between the additive particles and the sulfonic acid groups. In addition, an increase in intensity for the modified film can be seen, which can be attributed to the water retention effect of the LiF nanoparticles, similar to results in previous studies.[55] Under wet conditions, both membranes swell as expected and therefore form larger tunnel-like structures in the fully hydrated state, which is represented in a shift of the ionomer peak position to a smaller q-region. The data obtained from the calculated D-spacing for the water-equilibrated membranes is shown in Table S3. The value of the wet pristine membrane is 36.3 Å compared to 36.5 Å for the wet LiF(m), which corresponds to an increase in size during hydration of 6% and 12%, respectively. Considering the model of Schmidt-Rohr and Chen,[31] the diameters of the water channels are smaller than those calculated by the D-spacing. After wetting, the diameter increases from 22.9 to 24.2 Å for the pristine and from 21.7 to 24.4 Å for the modified membrane.

In contrast to previous observations, the intensity of the ionomer peak does not increase in the fully hydrated state in comparison to the dry samples.[54,56,57] These SAXS results support the previous water uptake studies presented here and indicate that the hygroscopic lithium fluoride nanoparticles can increase water uptake and retention.

3.3. Electrochemical Characterization. *Conductivity.* The influence of different lithium fluoride modifications and additive loadings on proton conductivity was studied under LT- and IT-PEM conditions on a commercial BekkTech cell (see 2.13 Proton conductivity measurements). Lithium fluoride concentrations of 4 wt % − 12 wt % were investigated, with the composite membrane with 10 wt % additive loading performing best at high temperatures (110 to 130 °C) and low RH (Figure 2b). Based on these proton conductivity results all further tests were performed with an optimized additive loading of 10 wt %.

Figure 8 shows the proton conductivities of the prepared membranes. Compared to the nonmodified 800EW sample, the commercial lithium fluoride membrane shows a con-
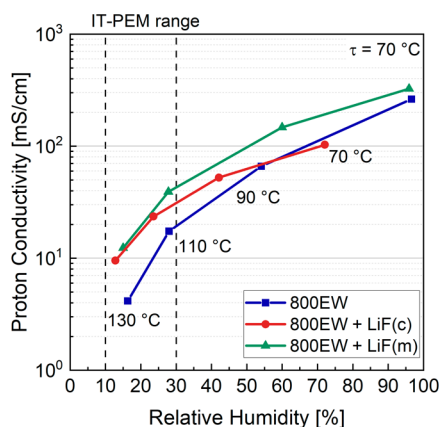
Figure 8. Proton conductivity measurements of the 800EW membrane, the LiF(c) and the LiF(m) composite membrane at various cell temperatures and relative humidities. A clear assignment of the measured conductivities to the corresponding temperatures can be found in SI: Figure S4.

ductivity increase observed at temperatures above 90 °C. The membrane with the milled nanolithium fluoride exhibits an increase in conductivity over the entire temperature range. Both composite membranes demonstrate increased proton conductivity values at 130 °C, directly within the IT-PEM temperature range. Nevertheless, the milled lithium fluoride sample with the smaller particle sizes showed a more pronounced improvement. From this, it can be concluded that smaller particle sizes and, consequently, a higher surface-to-volume ratio can increase the conductivity of the membrane. These results agree with the water uptake studies, in which the milled LiF modified membrane showed higher WU. For further measurements and fuel cell performance investigations, the focus was placed on milled lithium fluoride. However, polarization curves comparing commercial and milled LiF with the reference membrane are shown in Figure S8.

Fuel Cell Performance and Durability. The fuel cell performance of the manufactured membranes was validated by measuring polarization curves and performing accelerated stress tests (ASTs) at LT- and IT-PEM operating conditions (Figure S5 and Table S4 Please check: && S5). The parameters used focused primarily on moderate and dry

conditions in H_2-air mode to simulate the membrane's intermediate temperature applicability. The open circuit voltage (OCV) hold test was used to investigate the influence of the inorganic filler on the degradation behavior and the durability of the membranes under these harsh conditions.

Figure 9a shows the polarization curves as well as the power density curves of the pristine membrane and the LiF(m) modified membrane at LT-PEM conditions (80 °C & 50/30% RH). The first noticeable result is that the LiF(m) modified membrane has a higher maximum power density of 508 mW cm^{-2} compared to the unmodified membrane with only 380 mW cm^{-2}, which corresponds to an increase of 128 mW cm^{-2}. This clear advantage of the additive-modified membrane over the 800EW membrane is attributed to the following reasons: the water uptake increases due to the incorporation of the hygroscopic filler, seen for high relative humidity in Figure 6 and 7, which leads to an improved proton conductivity by retaining residual water at the additive/polymer interface (Figure 8).[43] Lithium fluoride's solubility under these conditions likely embeds it in smaller forms within the membrane, enabling hydrogen bonding between lithium ions and sulfonic acid groups. This interaction is expected to increase water retention, especially in low-humidity scenarios. Furthermore, a link between the sulfonic acid group and the additive can be assumed, like it was previously described for other hygroscopic filler systems such as $[R–SO_3H\cdots(SiO_2)]$.[26] The additives can stabilize the hydrophobic and hydrophilic domains by forming similar bridges $[R–SO_3H\cdots(LiF)]$, resulting in an increased T_g and higher mechanical stability (Figure 4(b)). Investigations by Singh et al.[58] demonstrated the same behavior for magnesium fluoride as an additive material. They analyzed the interaction between the PFSA and the filler system by vibrational spectroscopy, which indicated the dissociation of the acidic proton of the sulfonic acid group and, therefore, a strong bonding between the magnesium fluoride, the proton and the corresponding sulfonic acid group by strong hydrogen bonding.

This assumption is supported by the results obtained from the OCV holding tests (Figure S6c). The 800EW shows a constant decrease in potential during the OCV test. The voltage dropped by 6.5% from 939 mV (Begin of Test, BoT) down to 878 mV (End of Test, EoT). The lithium fluoride membrane, on the other hand, shows an almost constant potential curve. There is a minimal drop of 7 mV (0.6%)
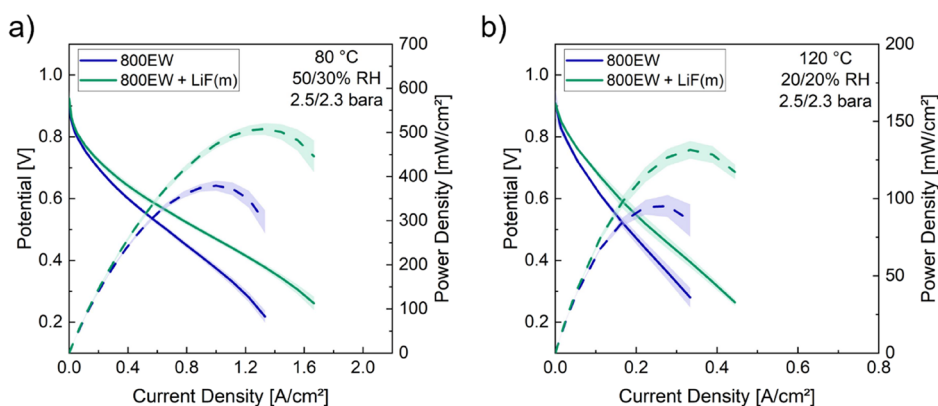

Figure 9. Polarization and power density curves of the pristine 800EW and the lithium fluoride membranes at 80 °C, 50/30% RH, 2.5/2.3 bara for anode/cathode (a) and at 120 °C, 20/20% RH, 2.5/2.3 bara for anode/cathode (b). Each curve represents the mean of at least three replicate measurements with the respective standard deviations indicated by the shaded areas.

during operation. Furthermore, it should be noted that the PPD loss after 120 h of OCV hold is only 12 mW cm^{-2} for the modified membrane (Table S6 Please check: && Figure S6b). The loss for the 800EW reference membrane is almost twice as high, with 22 mW cm^{-2}, at lower PPDs. The wavy shape of the OCV line in Figure S6c can be explained by the polarization curves measured every 24 h during the OCV hold test. This resulted in an increase in the open circuit voltage compared to the previous stage, which is due to a cleaning effect ("recovery") of the chemically poisoned membrane by the potential and current changes during the polarization curves.[59]

Figure 9b presents the polarization curves and power density curves at IT-PEM conditions at 120 °C and 20% RH. Compared to the tests at LT-PEM conditions, performed at lower temperatures and higher relative humidity, all MEAs showed a lower overall performance with maximum power densities up to 132 mW cm^{-2}. However, Figure 9b reveals a better overall performance for the lithium fluoride doped composite membrane. The PPD of the composite membrane reached 132 mW cm^{-2} compared to 95 mW cm^{-2} for the pristine membrane. This can be related to a better water retention and therefore higher proton conductivity with a decreased membrane resistance indicated by a flatter polarization curve in the ohmic resistance region. The high frequency resistance (HFR) measurements, recorded during the OCV hold test, corroborate this assumption with 142 mΩ cm^2 for the modified membrane and 165 mΩ cm^2 for the pristine one. A comparison of the polarization curves of the membrane modified with commercial lithium fluoride (LiF(c)) and the membranes presented in Figure 9b shows a similar peak power density of 130 mW cm^{-2} at 120 °C (Figure S8b). However, the membrane demonstrates a low OCV due to significant hydrogen crossover. This phenomenon is related to the formation of microdefects caused by the relatively large LiF particles, as shown in Figure S1.

The results of the OCV hold tests at IT-PEM conditions for the pristine and LiF(m) doped membrane are shown in Figure S7. The 800EW membrane showed a significantly higher OCV at the beginning of the measurement (985 mV). However, this dropped continuously, starting 1.5 h after BoT. After 15 h, the OCV dropped down to 836 mV, which corresponds to a voltage loss of 149 mV (95.33 mV h^{-1}). In contrast, the OCV of the LiF(m) modified membrane dropped only by 32 mV (11.46 mV h^{-1}) after 15 h from 925 mV (BoT) to 893 mV (EoL). For better comparison, the peak power density the decay rates and the HFR values of the pristine membrane and the LiF(m) composite membrane are given in Table S6.

Our newly developed lithium fluoride modified PFSA membranes demonstrated superior fuel cell performance compared to commercial membranes under similar conditions showing peak power densities of 508 mW cm^{-2} (80 °C, 50/30% RH, 2.5/2.3 bara) and 132 mW cm^{-2} (120 °C, 20/20% RH, 2.5/2.3 bara). Direct comparison of these membranes and other additive systems or membrane types are challenging due to significant differences in operating conditions, cell design, catalyst loadings, backpressure, and membrane materials, all of which have a significant impact on performance outcomes. Studies on additive-modified PFSA systems under elevated temperatures and reduced relative humidity demonstrate a broad range of PPD results, highlighting the influence of these parameters. Park et al.[60] achieved a high peak power density of 683 mW cm^{-2} (120 °C, 50% RH, 2 bara) using a binary oxide additive (ZrO$_2$−SiO$_2$). Similarly, Mazzapioda et al.[24] reported

a PPD of 105 mW cm^{-2} at 110 °C and 31% RH with a TiO$_2$−SO$_4$ additive. Other PEM fuel cell systems based on alternative approaches, such as cross-linked polymeric materials, sulfonated aromatic/hydrocarbon-based membranes, or polybenzimidazole (PBI) membranes, have demonstrated higher PPDs at extreme conditions (HT-PEM conditions), including temperatures up to 200 °C and very low humidity (≥0% RH). For example, Shang et al.[12] developed a poly(phenylene sulfonic acid)-based composite membrane that achieved a PPD of 850 mW cm^{-2} (80 °C, 30% RH, 2.0 bara). Similarly, Lim et al.[19] reported PPDs exceeding 600 mW cm^{-2} at 160 °C with no external humidification and approximately 1.5 bara backpressure using an ion-pair membrane doped with phosphoric acid. Currently these values cannot be rivaled with our approach, but one also has to keep in mind the difference in membrane thickness, which will also play a role. In the immediate future, one of the most important tasks in membrane development will be to obtain robust and thin membranes simultaneously.

4. CONCLUSION

In this article, μm-sized cubic lithium fluoride particles and their wet-milled nanosized analogues were incorporated into a PFSA composite membrane. Chemical and mechanical studies of the composite membranes were combined with a detailed electrochemical study to unravel the structure-performance relationship.

The embedded additive particles could increase the glass transition temperatures as shown by the DMA test, which can be explained by an interaction of the additives with the sulfonic acid groups. This assumption could be confirmed by SAXS measurements, where smaller hydrophilic domain sizes were observed for the composite membrane, indicating these molecular interactions. Furthermore, the interaction of the hygroscopic additives with water molecules through hydrogen bonds enhanced their water uptake, resulting in improved proton conductivity. The interplay between improved glass transition temperatures, increased water uptake and therefore improved proton conductivity led to enhanced fuel cell performance, as evidenced by higher power density values and increased stability in OCV hold tests at LT- and IT-PEMFC conditions. At IT-PEM conditions, the power density of the additive-modified membranes could be improved by up to 40% compared to the pristine membrane using wet-milled LiF nanoparticles.

In future work, mechanical testing and advanced and longer stress tests, e.g. by humidity cycling, should be done to investigate the membrane's behavior and stability further. In order to understand the influence of the LiF additive particles on phase separation and water retention and diffusion, we furthermore propose in situ SAXS and pulsed field gradient spin−echo (PGSE) NMR analysis under realistic operating conditions as well as computational simulations.[32,55,61,62] These studies will help to advance the composite membrane design further by tailoring the particle shapes, sizes, distribution and content toward optimal LT- and IT-performance.

AUTHOR INFORMATION

Corresponding Author

Maximilian Kutter − *Electrochemical Process Engineering, Universität Bayreuth, Bayreuth 95447, Germany; Keylab Glass Technology, Universität Bayreuth, Bayreuth 95447, Germany;* ⓘ orcid.org/0000-0002-5243-0817; Email: maximilian.kutter@uni-bayreuth.de

Authors

Annika Hilgert − *Electrochemical Process Engineering, Universität Bayreuth, Bayreuth 95447, Germany*

Maximilian Maier − *Helmholtz Institute Erlangen-Nürnberg for Renewable Energy (IET-2), Forschungszentrum Jülich GmbH, Erlangen 91058, Germany; Department of Chemical and Biological Engineering, Friedrich-Alexander-Universität Erlangen-Nürnberg, Erlangen 91058, Germany*

Monja Schilling − *Helmholtz Institute Ulm, Karlsruhe Institute of Technology, Ulm 89081, Germany*

Christopher R. Greve − *Dynamics and Structure Formation − Herzig Group, Institute of Physics, Universität Bayreuth, Bayreuth 95447, Germany;* ⓘ orcid.org/0000-0001-5506-9695

Rameshwori Loukrakpam − *Electrochemical Process Engineering, Universität Bayreuth, Bayreuth 95447, Germany*

Wiebke Hagemeier − *Electrochemical Process Engineering, Universität Bayreuth, Bayreuth 95447, Germany*

Andreas Rosin − *Keylab Glass Technology, Universität Bayreuth, Bayreuth 95447, Germany*

Mark Muggli − *3M Advanced Materials Division, Dyneon GmbH, Burgkirchen an der Alz 84508, Germany*

Eva M. Herzig − *Dynamics and Structure Formation − Herzig Group, Institute of Physics, Universität Bayreuth, Bayreuth 95447, Germany;* ⓘ orcid.org/0000-0002-0151-5562

Roswitha Zeis − *Helmholtz Institute Ulm, Karlsruhe Institute of Technology, Ulm 89081, Germany; Department of Mechanical & Industrial Engineering, University of Toronto, Toronto, ON M5S 3G8, Canada; Department of Electrical Electronics, and Communication Engineering, Friedrich-Alexander-Universität Erlangen-Nürnberg, Erlangen 91058, Germany;* ⓘ orcid.org/0000-0001-8379-0578

Thomas Böhm − *Helmholtz Institute Erlangen-Nürnberg for Renewable Energy (IET-2), Forschungszentrum Jülich GmbH, Erlangen 91058, Germany;* ⓘ orcid.org/0000-0003-2036-2159

Thorsten Gerdes − *Keylab Glass Technology, Universität Bayreuth, Bayreuth 95447, Germany*

Christina Roth − *Electrochemical Process Engineering, Universität Bayreuth, Bayreuth 95447, Germany;* ⓘ orcid.org/0000-0003-1159-2956

Author Contributions

Conceptualization, M.K., C.R., and T.G.; methodology, M.K., A.R., and A.H.; validation, M.K. and A.H.; formal analysis, M. K., A. H., M. M., C. G.; investigation, M.K., A.H., M.M., M.S., C.G., W.H.; resources, C.R., T.G., M.M.; data curation, M.K., A.R., R.L.; writing (original draft preparation), M.K., A.H., M.M., C.G., M.S.; writing (review and editing), M.K., M.M., T.B., R.Z., E.M.H., C.R.; visualization, M.K., A.H., M.M.; supervision, C.R., T.G., T.B.; project administration, M.K., C.R.; funding acquisition, C.R., T.G., T.B., R.Z., E.M.H., and M.M.

Notes

The authors declare the following competing financial interest(s): Maximilian Kutter has patent #Composite Including Fluorinated Polymer and Lithium Fluoride Nanoparticles and Articles Including the Same (WO2023/057926A1) licensed to 3M Innovative Properties Company.

REFERENCES

(1) Shin, S. H.; Nur, P. J.; Kodir, A.; Kwak, D. H.; Lee, H.; Shin, D.; Bae, B. Improving the Mechanical Durability of Short-Side-Chain Perfluorinated Polymer Electrolyte Membranes by Annealing and Physical Reinforcement. *ACS Omega* **2019**, *4*, 19153−19163.

(2) Kumar, R.; Xu, C.; Scott, K. Graphite Oxide/Nafion Composite Membranes for Polymer Electrolyte Fuel Cells. *RSC Adv.* **2012**, *2*, 8777−8782.

(3) Singh, R.; Oberoi, A. S.; Singh, T. Factors Influencing the Performance of PEM Fuel Cells: A Review on Performance Parameters, Water Management, and Cooling Techniques. *Int. J. Energy Res.* **2022**, *46*, 3810−3842.

(4) Gittleman, C. S.; Jia, H.; De Castro, E. S.; Chisholm, C. R. I.; Kim, Y. S. Proton Conductors for Heavy-Duty Vehicle Fuel Cells. *Joule* 2021, 5, 1660−1677.

(5) Rosli, R. E.; Sulong, A. B.; Daud, W. R. W.; Zulkifley, M. A.; Husaini, T.; Rosli, M. I.; Majlan, E. H.; Haque, M. A. A Review of High-Temperature Proton Exchange Membrane Fuel Cell (HT-PEMFC) System. *Int. J. Hydrogen Energy* 2017, 42, 9293−9314.

(6) Kakinuma, K.; Taniguchi, H.; Asakawa, T.; Miyao, T.; Uchida, M.; Aoki, Y.; Akiyama, T.; Masuda, A.; Sato, N.; Iiyama, A. The Possibility of Intermediate−Temperature (120 °C)−Operated Polymer Electrolyte Fuel Cells Using Perfluorosulfonic Acid Polymer Membranes. *J. Electrochem. Soc.* 2022, 169, No. 044522.

(7) Matos, B. R.; Dresch, M. A.; Santiago, E. I.; Moraes, L. P. R.; Carastan, D. J.; Schoenmaker, J.; Velasco-Davalos, I. A.; Ruediger, A.; Tavares, A. C.; Fonseca, F. C. Nafion Membranes Annealed at High Temperature and Controlled Humidity: Structure, Conductivity, and Fuel Cell Performance. *Electrochim. Acta* 2016, 196, 110−117.

(8) Mališ, J.; Paidar, M.; Bystron, T.; Brožová, L.; Zhigunov, A.; Bouzek, K. Changes in Nafion® 117 Internal Structure and Related Properties during Exposure to Elevated Temperature and Pressure in an Aqueous Environment. *Electrochim. Acta* 2018, 262, 264−275.

(9) Gloukhovski, R.; Freger, V.; Tsur, Y. Understanding Methods of Preparation and Characterization of Pore-Filling Polymer Composites for Proton Exchange Membranes: A Beginner's Guide. *Rev. Chem. Eng.* 2018, 34, 455−479.

(10) Arslan, F.; Chuluunbandi, K.; Freiberg, A. T. S.; Kormanyos, A.; Sit, F.; Cherevko, S.; Kerres, J.; Thiele, S.; Böhm, T. Performance of Quaternized Polybenzimidazole-Cross-Linked Poly(Vinylbenzyl Chloride) Membranes in HT-PEMFCs. *ACS Appl. Mater. Interfaces* 2021, 13, 56584−56596.

(11) Yandrasits, M.; Hamrock, S.; Grootaert, W.; Guerra, M.; Jing, N. Polymer Electrolyte Membranes Crosslinked by Nitrile Trimerization. US20050107489A1, 2003.

(12) Shang, Z.; Hossain, M. M.; Wycisk, R.; Pintauro, P. N. Poly(Phenylene Sulfonic Acid)-Expanded Polytetrafluoroethylene Composite Membrane for Low Relative Humidity Operation in Hydrogen Fuel Cells. *J. Power Sources* 2022, 535, No. 231375.

(13) Harun, N. A. M.; Shaari, N.; Nik Zaiman, N. F. H. A Review of Alternative Polymer Electrolyte Membrane for Fuel Cell Application Based on Sulfonated Poly(Ether Ether Ketone). *Int. J. Energy Res.* 2021, 45, 19671−19708.

(14) Nguyen, H.; Lombeck, F.; Schwarz, C.; Heizmann, P. A.; Adamski, M.; Lee, H. F.; Britton, B.; Holdcroft, S.; Vierrath, S.; Breitwieser, M. Hydrocarbon-Based Pemion™ Proton Exchange Membrane Fuel Cells with State-of-the-Art Performance. *Sustain. Energy Fuels* 2021, 5, 3687−3699.

(15) Savinell, R. F.; Litt, M. H. Proton Conducting Polymers Used as Membranes. US5525436A, 1996.

(16) Wang, J.-T.; Wainright, J.; Yu, H.; Litt, M.; Savinell, R. F. A H2/O2 Fuel Cell Using Acid Doped Polybenzimidazole as Polymer Electrolyte. *ECS Proc.* 1995, 1995−23, 202−213.

(17) Atanasov, V.; Lee, A. S.; Park, E. J.; Maurya, S.; Baca, E. D.; Fujimoto, C.; Hibbs, M.; Matanovic, I.; Kerres, J.; Kim, Y. S. Synergistically Integrated Phosphonated Poly(Pentafluorostyrene) for Fuel Cells. *Nat. Mater.* 2021, 20, 370−377.

(18) Lee, K. S.; Spendelow, J. S.; Choe, Y. K.; Fujimoto, C.; Kim, Y. S. An Operationally Flexible Fuel Cell Based on Quaternary Ammonium-Biphosphate Ion Pairs. *Nat. Energy* 2016, 1, 16120.

(19) Lim, K. H.; Matanovic, I.; Maurya, S.; Kim, Y.; De Castro, E. S.; Jang, J. H.; Park, H.; Kim, Y. S. High Temperature Polymer Electrolyte Membrane Fuel Cells with High Phosphoric Acid Retention. *ACS Energy Lett.* 2023, 8, 529−536.

(20) Jalani, N. H.; Dunn, K.; Datta, R. Synthesis and Characterization of Nafion®-MO2 (M = Zr, Si, Ti) Nanocomposite Membranes for Higher Temperature PEM Fuel Cells. *Electrochim. Acta* 2005, 51, 553−560.

(21) Adjemian, K. T.; Dominey, R.; Krishnan, L.; Ota, H.; Majsztrik, P.; Zhang, T.; Mann, J.; Kirby, B.; Gatto, L.; Velo-Simpson, M.; Leahy, J.; Srimvasan, S.; Benziger, J. B.; Bocarsly, A. B. Function and Characterization of Metal Oxide-Nafion Composite Membranes for Elevated-Temperature H 2/O 2 PEM Fuel Cells. *Chem. Mater.* 2006, 18, 2238−2248.

(22) Alberti, G.; Casciola, M.; Capitani, D.; Donnadio, A.; Narducci, R.; Pica, M.; Sganappa, M. Novel Nafion−Zirconium Phosphate Nanocomposite Membranes with Enhanced Stability of Proton Conductivity at Medium Temperature and High Relative Humidity. *Electrochim. Acta* 2007, 52, 8125−8132.

(23) Bauer, F.; Willert-Porada, M. Comparison between Nafion® and a Nafion® Zirconium Phosphate Nano-Composite in Fuel Cell Applications. *Fuel Cells* 2006, 6, 261−269.

(24) Mazzapioda, L.; Panero, S.; Navarra, M. A. Polymer Electrolyte Membranes Based on Nafion and a Superacidic Inorganic Additive for Fuel Cell Applications. *Polymers (Basel).* 2019, 11, 914.

(25) Di Noto, V.; Piga, M.; Piga, L.; Polizzi, S.; Negro, E. New Inorganic−Organic Proton Conducting Membranes Based on Nafion® and [(ZrO2)·(SiO2)0.67] Nanoparticles: Synthesis Vibrational Studies and Conductivity. *J. Power Sources* 2008, 178, 561−574.

(26) Di Noto, V.; Gliubizzi, R.; Negro, E.; Pace, G. Effect of SiO2 on Relaxation Phenomena and Mechanism of Ion Conductivity of [Nafion/(SiO2)x] Composite Membranes. *J. Phys. Chem. B* 2006, 110, 24972−24986.

(27) Gierke, T. D.; Munn, G. E.; Wilson, F. C. The Morphology in Nafion Perfluorinated Membrane Products, as Determined by Wide- and Small-Angle x-Ray Studies. *J. Polym. Sci. Polym. Phys. Ed.* 1981, 19, 1687−1704.

(28) Hsu, W. Y.; Gierke, T. D. Ion Transport and Clustering in Nafion Perfluorinated Membranes. *J. Membr. Sci.* 1983, 13, 307−326.

(29) Fujimura, M.; Hashimoto, T.; Kawai, H. Small-Angle X-Ray Scattering Study of Perfluorinated Ionomer Membranes. 1. Origin of Two Scattering Maxima. *Macromolecules* 1981, 14, 1309−1315.

(30) Gebel, G. Structural Evolution of Water Swollen Perfluorosulfonated Ionomers from Dry Membrane to Solution. *Polymer (Guildf).* 2000, 41, 5829−5838.

(31) Schmidt-Rohr, K.; Chen, Q. Parallel Cylindrical Water Nanochannels in Nafion Fuel-Cell Membranes. *Nat. Mater.* 2008, 7, 75−83.

(32) Kusoglu, A.; Dursch, T. J.; Weber, A. Z. Nanostructure/ Swelling Relationships of Bulk and Thin-Film PFSA Ionomers. *Adv. Funct. Mater.* 2016, 26, 4961−4975.

(33) Moszczynska, A.; Wolf, H.; Willert-Porada, M. A. Cation Conductive Membranes Comprising Polysulfonic Acid Polymers and Metal Salts Having an F-Containing Anion. WO 2009/014930, 2008.

(34) Kutter, M.; Greve, C.; Maier, M.; Schilling, M.; Mauel, A.; Hilgert, A.; Hoffmann, H.; Hagemeier, W.; Rosin, A.; Muggli, M.; Zeis, R.; Senker, J.; Böhm, T.; Herzig, E. M.; Gerdes, T.; Roth, C. Recycling of Perfluorosulfonic Acid-Based Membranes and Their Re-Application in PEM Fuel Cells. *J. Membr. Sci.* 2024, 693, No. 122370.

(35) Wall, C.; Pohl, A.; Knapp, M.; Hahn, H.; Fichtner, M. Production of Nanocrystalline Lithium Fluoride by Planetary Ball-Milling. *Powder Technol.* 2014, 264, 409−417.

(36) Peng, Z.; Huguet, P.; Deabate, S.; Morin, A.; Sutor, A. K. Depth-Resolved Micro-Raman Spectroscopy of Tri-Layer PFSA Membrane for PEM Fuel Cells: How to Obtain Reliable Inner Water Contents. *J. Raman Spectrosc.* 2013, 44, 321−328.

(37) Böhm, T.; Moroni, R.; Breitwieser, M.; Thiele, S.; Vierrath, S. Spatially Resolved Quantification of Ionomer Degradation in Fuel Cells by Confocal Raman Microscopy. *J. Electrochem. Soc.* 2019, 166, F3044−F3051.

(38) Maier, M.; Abbas, D.; Komma, M.; Mu'min, M. S.; Thiele, S.; Böhm, T. A Comprehensive Study on the Ionomer Properties of PFSA Membranes with Confocal Raman Microscopy. *J. Membr. Sci.* 2023, 669, No. 121244.

(39) Heimerdinger, P.; Rosin, A.; Danzer, M. A.; Gerdes, T. A Novel Method for Humidity-Dependent Through-Plane Impedance Measurement for Proton Conducting Polymer Membranes. *Membranes (Basel).* 2019, 9, 62.

(40) Alharbi, N. D.; Salah, N.; Habib, S. S.; Alarfaj, E. Synthesis and Characterization of Nano- and Microcrystalline Cubes of Pure and Ag-Doped LiF. *J. Phys. D. Appl. Phys.* **2013**, *46*, No. 035305.

(41) Giffin, G. A.; Haugen, G. M.; Hamrock, S. J.; Di Noto, V. Interplay between Structure and Relaxations in Perfluorosulfonic Acid Proton Conducting Membranes. *J. Am. Chem. Soc.* **2013**, *135*, 822−834.

(42) Deng, Q.; Wilkie, C. A.; Moore, R. B.; Mauritz, K. A. TGA−FTi.r. Investigation of the Thermal Degradation of Nafion® and Nafion®/[Silicon Oxide]-Based Nanocomposites. *Polymer (Guildf).* **1998**, *39*, 5961−5972.

(43) Noto, V. Di; Piga, M.; Negro, E.; Giffin, G. A.; Polizzi, S.; Zawodzinski, T. A. New Nanocomposite Proton Conducting Membranes Based on a Core−Shell Nanofiller for Low Relative Humidity Fuel Cells. *RSC Adv.* **2013**, *3*, 18960−18969.

(44) Luo, X.; Lau, G.; Tesfaye, M.; Arthurs, C. R.; Cordova, I.; Wang, C.; Yandrasits, M.; Kusoglu, A. Thickness Dependence of Proton-Exchange-Membrane Properties. *J. Electrochem. Soc.* **2021**, *168*, No. 104517.

(45) Kollath, V. O.; Liang, Y.; Mayer, F. D.; Ma, X.; Korzeniewski, C.; Karan, K. Model-Based Analyses of Confined Polymer Electrolyte Nanothin Films Experimentally Probed by Polarized ATR−FTIR Spectroscopy. *J. Phys. Chem. C* **2018**, *122*, 9578−9585.

(46) Gruger, A.; Régis, A.; Schmatko, T.; Colomban, P. Nanostructure of Nafion® Membranes at Different States of Hydration: An IR and Raman Study. *Vib. Spectrosc.* **2001**, *26*, 215−225.

(47) Korzeniewski, C.; Liang, Y.; Zhang, P.; Sharif, I.; Kitt, J. P.; Harris, J. M.; Hamrock, S. J.; Creager, S. E.; DesMarteau, D. D. Vibrational Spectroscopy for the Determination of Ionizable Group Content in Ionomer Materials. *Appl. Spectrosc.* **2018**, *72*, 141−150.

(48) Danilczuk, M.; Lin, L.; Schlick, S.; Hamrock, S. J.; Schaberg, M. S. Understanding the Fingerprint Region in the Infra-Red Spectra of Perfluorinated Ionomer Membranes and Corresponding Model Compounds: Experiments and Theoretical Calculations. *J. Power Sources* **2011**, *196*, 8216−8224.

(49) Chourdakis, N.; Voyiatzis, G. A. Molecular Orientation Study of Uniaxially Drawn Nafion Polymer Electrolyte Membranes Utilizing Polarized UV−Raman Spectra. *J. Polym. Sci., Part B: Polym. Phys.* **2007**, *45*, 2509−2517.

(50) Bribes, J. -L; El Boukari, M.; Maillols, J. Application of Raman Spectroscopy to Industrial Membranes. Part 2−Perfluorosulphonic Membrane. *J. Raman Spectrosc.* **1991**, *22*, 275−279.

(51) Kusoglu, A.; Weber, A. Z. New Insights into Perfluorinated Sulfonic-Acid Ionomers. *Chem. Rev.* **2017**, *117*, 987−1104.

(52) Rubatat, L.; Rollet, A. L.; Gebel, G.; Diat, O. Evidence of Elongated Polymeric Aggregates in Nafion. *Macromolecules* **2002**, *35*, 4050−4055.

(53) Mauritz, K. A.; Moore, R. B. State of Understanding of Nafion. *Chem. Rev.* **2004**, *104*, 4535−4585.

(54) Liu, Y.; Horan, J. L.; Schlichting, G. J.; Caire, B. R.; Liberatore, M. W.; Hamrock, S. J.; Haugen, G. M.; Yandrasits, M. A.; Seifert, S.; Herring, A. M. A Small-Angle X-Ray Scattering Study of the Development of Morphology in Films Formed from the 3M Perfluorinated Sulfonic Acid Ionomer. *Macromolecules* **2012**, *45*, 7495−7503.

(55) Niu, J.; Zhang, S.; Li, Y.; Li, X.; Zhang, J.; Lu, S.; He, Q. Effects of Microstructure on the Retention of Proton Conductivity of Nafion/SiO2 Composite Membranes at Elevated Temperatures:An in Situ SAXS Study. *Polymer (Guildf).* **2023**, *273*, No. 125869.

(56) Roche, E. J.; Pineri, M.; Duplessix, R.; Levelut, A. M. Small-Angle Scattering Studies of Nafion Membranes. *J. Polym. Sci. Polym. Phys. Ed.* **1981**, *19*, 1−11.

(57) Kusoglu, A.; Savagatrup, S.; Clark, K. T.; Weber, A. Z. Role of Mechanical Factors in Controlling the Structure-Function Relationship of PFSA Ionomers. *Macromolecules* **2012**, *45*, 7467−7476.

(58) Singh, B.; Singh, M.; Willert-Porada, M. Investigation of the Coupled Effect of Liquid and Solid Inorganic Additives on Thermal Stability and Water Retention of PFSA Composite. *J. Phys. Chem. C* **2018**, *122*, 9169−9183.

(59) Choi, S. R.; Kim, D. Y.; An, W. Y.; Choi, S.; Park, K.; Yim, S. D.; Park, J. Y. Assessing the Degradation Pattern and Mechanism of Membranes in Polymer Electrolyte Membrane Fuel Cells Using Open-Circuit Voltage Hold and Humidity Cycle Test Protocols. *Mater. Sci. Energy Technol.* **2022**, *5*, 66−73.

(60) Park, K. T.; Jung, U. H.; Choi, D. W.; Chun, K.; Lee, H. M.; Kim, S. H. ZrO2-SiO2/Nafion® Composite Membrane for Polymer Electrolyte Membrane Fuel Cells Operation at High Temperature and Low Humidity. *J. Power Sources* **2008**, *177*, 247−253.

(61) Shi, S.; Weber, A. Z.; Kusoglu, A. Structure/Property Relationship of Nafion XL Composite Membranes. *J. Membr. Sci.* **2016**, *516*, 123−134.

(62) Filipoi, C.; Demco, D. E.; Zhu, X.; Vinokur, R.; Conradi, O.; Fechete, R.; Möller, M. Channel Orientation Anisotropy in Perfluorosulfonic Acid/SiO2 Composite Proton Exchange Membranes: Water Self-Diffusion Study Using NMR. *Chem. Phys. Lett.* **2011**, *513*, 251−255.